

2022

Load Sharing Assessment of Osseoligamentous Structures Within a Thoracic Spine Segment During Surgical Release

Michael Polanco
Old Dominion University, mpolanco@odu.edu

James Bennett
Children's Hospital of the Kings Daughters

Austin Tapp
Old Dominion University

Michel Audette
Old Dominion University, maudette@odu.edu

Stacie Ringleb
Old Dominion University, sringleb@odu.edu

See next page for additional authors

Follow this and additional works at: https://digitalcommons.odu.edu/ece_fac_pubs



Part of the [Biomedical Engineering and Bioengineering Commons](#), [Musculoskeletal System Commons](#), and the [Surgery Commons](#)

Original Publication Citation

Polanco, M., Bennett, J., Tapp, A., Audette, M., Ringleb, S., & Bawab, S. (2022). *Load sharing assessment of osseoligamentous structures within a thoracic spine segment during surgical release*. Research Square. <https://doi.org/10.21203/rs.3.rs-2214576/v1>

This Article is brought to you for free and open access by the Electrical & Computer Engineering at ODU Digital Commons. It has been accepted for inclusion in Electrical & Computer Engineering Faculty Publications by an authorized administrator of ODU Digital Commons. For more information, please contact digitalcommons@odu.edu.

Authors

Michael Polanco, James Bennett, Austin Tapp, Michel Audette, Stacie Ringleb, and Sebastian Bawab

Load sharing assessment of osseoligamentous structures within a thoracic spine segment during surgical release

Michael Polanco¹, James Bennett², Austin Tapp³, Michel Audette³, Stacie Ringleb¹ and Sebastian Bawab^{1*}

^{1*}Mechanical and Aerospace Engineering, Old Dominion University, Norfolk, VA, 23529, USA.

² Children's Hospital of the King's Daughters, Norfolk, VA, 23507, USA.

³Biomedical Engineering, Old Dominion University, Norfolk, VA, 23529, USA.

*Corresponding author(s). E-mail(s): sbawab@odu.edu;
Contributing authors: mpola002@odu.edu;
james.t.bennett@gmail.com; atapp001@odu.edu;
maudette@odu.edu; sringleb@odu.edu;

Abstract

Spinal surgical procedures often require release of intervertebral discs and ligaments to optimally achieve postural correction on a patient-specific basis. In this paper, a T7-T8 Finite Element (FE) model is utilized to examine internal load sharing during resection steps performed in a Ponte osteotomy. The FE model was rotated bidirectionally along three anatomical planes using an externally applied moment. In each step, the Ranges of Motion (RoM), Instantaneous Centers of Rotation (ICR), and forces from ligaments, discs, facet, and costovertebral joints were calculated. The product of each component's force and the distance between the ICR and their position were used to calculate percent load sharing at the maximum moment magnitude. Removal of the facet joints accounts for overall significant increases in load sharing to the intervertebral disc, with maximum values reported in extension by approximately 18 percent and axial rotation by 16 percent. This study highlights key spine components whose kinematic influence may be considered to achieve desired surgical outcomes.

Keywords: scoliosis, finite element modeling, thoracic spine, load sharing, instantaneous center of rotation

1 Introduction

Adolescent Idiopathic Scoliosis (AIS) is a three-dimensional deformity of the spine that affects approximately 2.5 percent of patients aged 10-18; approximately 10 percent of those patients will require surgical intervention to prevent progression of the deformity (Asher and Burton 2006). Release procedures for spinal correction traditionally require the removal of osseoligamentous (bone and ligaments) anatomy to achieve sufficient correction. The sequential steps that a surgeon performs for spinal correction and fusion depend upon experience level (Majdouline et al 2009), the deformity profile and apex location (Lenke et al 2003), and curve flexibility, which is influenced by soft tissue and vertebral morphology (He and Wong 2018; Little and Adam 2011a). Historically, anterior-based releases of the spinal column were done to help achieve correction. However, posterior-based spinal surgery has allowed for improved 3-column correction of the spine with procedures such as the Ponte osteotomy (Samdani et al 2015).

In-vitro experiments that serially remove ligaments, facets (Heuer et al 2007; Wilke et al 2020), ribs, and costovertebral (CV) joints (Oda et al 2002; Liebsch and Wilke 2020) offer insight into spinal kinematics. However, experimental results do not provide information on load distribution changes within the spine following component removal. A load distribution assessment through Finite Element (FE) modeling may help surgeons understand how soft tissue components behave after serial release or vertebral fusions and could lead to improved patient outcomes. FE models of the spinal column have been utilized as a powerful non-invasive tool to answer clinical questions regarding scoliosis (Wang et al 2014). Additionally, FE models can examine the biomechanical effects of non-surgical treatment options and surgical steps prior to implementation (Lafon et al 2010; Vergari et al 2015).

Load distribution through FE analysis has been used to understand the role of ligaments and facets on rotational stability of the lumbar spine (Sharma et al 1995) and the cervical spine (Panzer and Cronin 2009) during release. Recent efforts have assessed load distribution in lumbar spine components to evaluate post-surgical treatment effectiveness of interbody spinal fusions (Zhang et al 2018) and interspinous process device designs (Lo et al 2020). Additionally, static equilibrium equations have been used to quantify and assess sagittal load sharing among osseoligamentous entities in an intact lumbosacral spine (Naserkhaki et al 2016). Yet, little is presently known about the load distribution of the thoracic spine during motion. The thoracic column is a common site for hyperkyphotic and scoliotic deformity and, because of the connections of the ribs to vertebrae via CV joints, this area of the spine is provided reinforcement and stability not seen in the cervical and lumbar regions. A study by

Little and Adam (2011b) previously explored the effect of CV joint incorporation on the load distribution of posterior ligaments within a thoracic functional unit. However, their study was primarily guided by validating their FE model with in vitro experimental data (Oda et al 2002), focusing on anterior release procedures and fixing the axis of rotation about the mid-column according to experimental conditions.

As previously recommended (Little and Adam 2011b), loading must take place about an Instantaneous Center of Rotation (ICR) to accurately represent physiological joint motion and predict load distribution and deformations about the spinal column (Schmidt et al 2008; Shirazi-Adl et al 1986). The ICR has been previously studied in FE models to understand the role spinal ligaments play in stabilizing a damaged thoracolumbar spine during resectioning (Wu et al 2018). An ICR assessment for the thoracic spine could guide appropriate surgical treatments for patients with scoliosis. The following study examines the effect of load distribution within the osseoligamentous components of a thoracic functional unit during posterior release and as a function of ICR.

2 Methods

A T7-T8 FE model (Figure 1a) was constructed from an anatomist-drawn computer aided design (CAD)-based spine model whose morphology is representative of an asymptomatic adult (CG Hero Ltd., Manchester, UK). The T7-T8 segment was tessellated using Hypermesh (Altair Engineering, Troy, MI, USA). Both vertebrae consisted of superior and inferior endplates, represented by quadrilateral elements, cortical bone, represented by quadrilateral and triangular elements, and cancellous bone, represented by hexahedral elements. Both the vertebral arch and spinous process, which are connected posteriorly to the cancellous bone, were represented using tetrahedral elements. Material properties for all components were acquired from literature (Table 1). The intervertebral disc (IVD) components (Figure 1b), the annulus fibrosus and nucleus pulposus, were both represented using hexahedral elements. The transverse cross-sectional area and the volume of the nucleus pulposus relative to the intervertebral disc were approximately 37 and 40 percent respectively (Table 2). Fibers within the annulus fibrosus were represented using cables and configured such that their total volume equated to approximately 16 percent of the ground substance; geometric (e.g., cross-sectional area) and material property scale factors for the fibers were configured (Table 3) (Shirazi-Adl et al 1986) for the IVD containing 8 radial layers and 3 layers through the thickness. A frictionless penalty contact algorithm was employed to represent the facet capsule, using contact thickness values to facilitate a 0.5mm initial gap between superior and inferior facet processes. This algorithm was also employed on rib sections to represent contact between the rib and the functional unit, facilitated by null contact elements over the ribs. In total, the FE model contains 34,990 elements and 15,944 nodes.

Seven intervertebral ligament groups (Table 4) were included within the functional unit configuration. Each ligament group's force-displacement properties (Figure 2) were derived from uniaxial stress-strain curves by respectively using the cross-sectional area and the initial ligament lengths as scale factors. Cross-sectional areas documented for the mid-thoracic region (Chazal et al 1985) were averaged and evenly distributed to all ligaments in each group; a cross-sectional area for the lumbar region was assumed for the capsular ligament due to absent data (Shirazi-Adl et al 1986). The CV joint was also incorporated to bilaterally connect 3cm of rib to the functional unit. The CV joint consisted of two separate joint groups (Figure 1c): the Costocentral joint (CCJ), consisting of the Intra-articular and Radiate ligaments, which connect the rib head to the spinal column, and the Costotransverse joint (CTV), consisting of the Lateral Costotransverse, Superior Costotransverse and Costotransverse ligaments, which connect the ribs to adjacent transverse processes. Uniaxial effective stiffness properties for CV joint ligaments utilized are listed in Table 5. All intervertebral and CV joint ligaments considered utilized tension-only elements.

Quasi-static analyses on the functional unit were performed using LS-DYNA implicit SMP Version 971 R10.1 (Livermore Software Technology, Livermore, CA, USA). To validate the ligament property set utilized in this study, a stepwise ligament removal procedure was first simulated on the functional unit based on the experimental conditions from Wilke et al (2020). Throughout the procedure, the unit was rotated in flexion, extension, right lateral bending, and left axial rotation. By including only one half of rotations in the coronal and axial planes, symmetry behavior was assumed. Range of Motion (RoM) data during each step was collected from the T7 superior endplate using a local coordinate system defined per the Scoliosis Research Society recommendations (Stokes et al 1994). A pure moment of ± 2.5 N-m and no preload was employed for all cases. The T8 inferior endplate and facet processes were fixed. Per the experiment, the following configurations were analyzed sequentially: Intact, Supraspinous Ligament (SSL) removal, Interspinous Ligament (ISL) removal, Ligamentum Flavum (LF) removal, and Facet Joint (FJ) removal, the latter referring to the capsular ligament and facet capsule combined. Based on specimen conditions during experimentation, the CV joint and ITL were excluded from this procedure. CV joint kinematics were previously validated in comparison with in-vitro data (Polanco et al 2022).

Next, the resection procedure consistent with a Ponte osteotomy was implemented onto the functional unit model. Per the standard recommended moments to be applied to thoracic spine segments in-vitro (Wilke et al 1998), a ± 5 N-m pure moment with no preload was applied over the superior T7 endplate. The unit was rotated in flexion, extension, left and right lateral bending, and left and right axial rotation. For each rotation direction, five different configurations were assessed to represent the steps of the Ponte osteotomy as follows (Figure 3):

- (1) all spine components intact,
- (2) removal of the interspinous and supraspinous ligaments,
- (3) bilateral inferior facetectomy,
- (4) removal of the ligamentum flavum, and
- (5) completion of the osteotomy across the superior facet.

During each analysis, the following assumptions were made: approximately two-thirds of each facet surface and all capsular ligaments were symmetrically removed by the bilateral inferior facetectomy. Secondly, because ligaments primarily control rotational behavior of the functional unit, bones serving as ligament attachments were not removed during each step of the osteotomy. Finally, as with the previous study, the T8 inferior endplate and facet processes were fixed. In each step, the RoM was calculated using vector projection along the superior endplate. The ICR trace along the rotational plane was calculated based on the perpendicular bisector method (Pearcy and Bogduk 1998). The ICR location (Figure 4) was used to find the moment arm for each spinal component and was multiplied by forces calculated in the analyses for all ligaments, intervertebral discs, and joints. Using Equation 1, rotational equilibrium was assumed in all cases to calculate the moment distribution for each component about the ICR. The moment distributions were calculated as percentages of the externally applied moment. Ligament, disc, and facet force information can be found in supplementary material.

$$\sum M_{ICR} = \overrightarrow{M_{External}} + \sum (\overrightarrow{r_{(ICR-LigamentPosition)}} * \overrightarrow{F_{Ligament}}) + \sum (\overrightarrow{r_{(ICR-JointPosition)}} * \overrightarrow{F_{joint}}) + (\overrightarrow{M_{Disc}}) = 0 \quad (1)$$

Table 1: Intervertebral joint material properties

Spinal Component	Material Constitutive Model	Material Property	Source
Cortical Bone	Linear Elastic	E=12 GPa, ν=0.3	Naserkhaki et al 2018
Cancellous Bone	Linear Elastic	E=200 MPa, ν=0.315	Naserkhaki et al 2018
Rib	Linear Elastic	E=12 GPa, ν=0.35	Schlager et al 2018
Endplate ¹	Linear Elastic	E=23.8 MPa, ν=0.4	Schmidt et al 2006
Annulus Fibrosus	Mooney-Rivlin	C10=0.18 MPa,	Schmidt et al 2006
	Hyperelastic	C01=0.045 MPa, ν=0.45	
Nucleus Pulposus	Mooney-Rivlin	C10=0.12 MPa,	Schmidt et al 2006
	Hyperelastic	C01=0.03 MPa, ν=0.499	

¹ 1mm thickness

Table 2: Intervertebral Disc dimensions

Anterior (mm)	Center (mm)	Posterior (mm)	Nucleus Pulposus Cross- Sectional Area (mm ²)	Nucleus Pulposus Volume (mm ³)	Transverse Disc Cross- Sectional Area (mm ²)	Disc Volume (mm ³)
5.9	6.9	4.8	352	1242	1049.5	3073

Table 3: Geometric and material scale factors for annulus fibers

	Layers 1 and 2	Layers 3 and 4	Layers 5 and 6	Layers 7 and 8
Geometric ¹	1	0.78	0.62	0.47
Material ¹	1	0.9	0.75	0.65

¹Scale factors taken from Shirazi-Adl et al (1986)

Table 4: Average model ligament lengths and cross-sectional areas

Spinal Component	Average length (mm)	Average Cross- Sectional Areas (mm ²)	Source ¹
Anterior Longitudinal Ligament (ALL)	5.36	30	Chazal et al 1985
Posterior Longitudinal Ligament (ALL)	4.929	17	Chazal et al 1985
Ligamentum Flavum (LF)	24.832	26.7	Chazal et al 1985
Interspinous Ligament (ISL)	5.541	30	Chazal et al 1985
Supraspinous Ligament (SSL)	25.588	30	Chazal et al 1985
Capsular Ligament (CL)	2.799 (over both sides)	36	Shirazi-Adl et al 1986
Intertransverse Ligament (ITL)	18.326 (over both sides)	1.85	Chazal et al 1985

¹Cross-sectional area values

3 Results

3.1 FE Model Validation-Stepwise Ligament removal

The largest RoM increases relative to the preceding removal step (Figure 5) come after both the ligamentum flavum and the facet joint are removed in flexion, respectively at approximately 154 percent and 28 percent at 1 N-m and 50 percent and 77 percent at 2.5 N-m. Negligible increases in overall RoM were seen within removal steps exercised in extension, right lateral bending,

Table 5: Costovertebral Joint properties

Spinal Component	Material Property	Source
Lateral Costotransverse Ligament (LCTL)	$K_{eff} = 126.5N/mm$	Aira et al 2019
Superior Costotransverse Ligament (SCTL)	$K_{eff} = 90.2N/mm$	Aira et al 2019
Costotransverse Ligament (CTL)	$K_{eff} = 54.9N/mm$	Aira et al 2019
Radiate Ligament	$A=10mm^2, E = 42.1MPa$	Aira et al 2019 Jiang et al 1994
Intra-articular Ligament	$K_{eff} = 20.9N/mm$	Aira et al 2019

and left axial rotation; the maximum was 3.7 percent after facet removal in extension. The extension modes were compliant compared to the experimental data; however, most of the ligament removal steps in flexion, right lateral bending and left axial rotation were within range of the data highlighted from the experiment. Since most of the RoM data was within range of the experimental data, the ligament properties were deemed acceptable for further use.

3.2 RoM and ICR kinematic assessment

Next, the functional unit with both the ITL and the CV joint incorporated were rotated along the three anatomical planes. The RoM (Figure 6) increase during serial ligament removal in flexion amounted to approximately 18 percent, 1.4 percent, and 11.9 percent for the spinous ligament, bilateral inferior facetectomy, and ligamentum flavum removal stages, respectively. No change was seen after the bilateral superior facetectomy was conducted. After the inferior facets were removed, RoM increased in extension by 16 percent, in left axial rotation by 12.1 percent, in right axial rotation by 10.7 percent and in left lateral bending by 2.5 percent. Following the bilateral superior facetectomy, a 0.8 percent increase in RoM was seen in right lateral bending. When the superior facets were removed, the RoM overall showed no more than a 1.5 percent increase; the maximum increase took place in right axial rotation.

In flexion (Figure 7a), at the maximum applied moment, the removal of the spinous ligaments shifts the ICR anteriorly by 0.97mm and superiorly by 3.72mm. In the same circumstance, after the bilateral inferior facetectomy, the ICR is shifted anteriorly by 0.27mm and superiorly by 1.14mm. After the ligamentum flavum is removed, the ICR shifts 2mm anteriorly and 0.82mm superiorly. No changes were seen after the bilateral superior facetectomy. In extension after the bilateral inferior facetectomy, anterior and inferior ICR shifts of 0.11mm and 0.71mm were respectively observed. In extension after the bilateral superior facetectomy, superior direction ICR shifts of 0.23mm were observed; a negligible shift in the anterior direction was observed. The ICR position in left and right lateral bending (Figure 7b) overall see a negligible shift upon all steps and directions in ligament removal (less than 0.1mm). In

Table 6: Load distribution percent by spine component at maximum sagittal moment (5 N-m)

		ALL	CCJ	CTV	FJ	IVD	ITL	LF	ISL	SSL	PLL
Intact	Flexion	0	0.05	4.2	1.9	43.9	16.7	15.6	8.6	9.1	0
	Extension	0.42	4.2	7.5	22.2	65.7	0	0	0	0	0
ISL and SSL removed	Flexion	0	0.62	4.7	3.2	48.6	22.1	20.8	0	0	0
	Extension	0.42	4.2	7.5	22.2	65.6	0	0	0	0	0
Bilateral Inferior Facetectomy	Flexion	0	1	4.6	0	48.5	24.1	21.8	0	0	0
	Extension	0.47	5.8	9.9	0.4	83.5	0	0	0	0	0
LF removed	Flexion	0	1.4	5.8	0	47.3	45.5	0	0	0	0
	Extension	0.47	5.8	9.9	0.4	83.5	0	0	0	0	0
Bilateral Superior Facetectomy	Flexion	0	1.5	5.8	0	47.3	45.5	0	0	0	0
	Extension	0.47	5.7	10.0	0	83.8	0	0	0	0	0

Table 7: Load distribution percent by spine component at maximum coronal moment (5 N-m)

		CCJ- Left	CCJ- Right	CTV- Left	CTV- Right	FJ- Left	FJ- Right	ITL- Left	ITL- Right	IVD
Intact	Left	2.8	0.47	3.6	3.5	2.5	0	0	7.6	79.4
	Right	0.28	12.6	2.5	6.8	0	1.4	6.2	0	70.2
ISL and SSL removed	Left	2.8	0.47	3.7	3.5	2.5	0	0	7.6	79.4
	Right	0.28	12.6	2.5	6.8	0	1.4	6.2	0	70.2
Bilateral Inferior Facetectomy	Left	3.1	0.44	4.1	3.4	0	0	0	7.2	81.6
	Right	0.28	12.6	2.5	6.8	0	1.4	6.2	0	70.2
LF removed	Left	3.1	0.44	4.1	3.4	0	0	0	7.2	81.6
	Right	0.28	12.6	2.5	6.8	0	1.4	6.2	0	70.1
Bilateral Superior Facetectomy	Left	3.1	0.44	4.1	3.4	0	0	0	7.2	81.6
	Right	0.32	11.7	2.6	6.3	0	0	6.1	0	73.1

Table 8: Load distribution percent by spine component at maximum axial moment (5 N-m)

		CCJ- Left	CCJ- Right	CTV- Left	CTV- Right	FJ- Left	FJ- Right	ISL	ITL- Left	ITL- Right	IVD
Intact	Left	1.7	3.6	6.4	6	14.1	3.6	0	0	0.97	63.7
	Right	0.92	6	2	2.8	14.4	5.8	0.64	0.42	0	67.1
ISL and SSL removed	Left	1.7	3.6	6.4	5.9	14.2	3.6	0	0	0.98	63.7
	Right	0.95	6	2.1	2.8	14.3	6.1	0	0.63	0	67.2
Bilateral Inferior Facetectomy	Left	2.2	4	7.9	6.6	0	1.4	0	0	1.6	76.4
	Right	1.1	7.5	4	3.1	4.6	0	0	1.1	0	78.5
LF removed	Left	2.2	4	7.9	6.6	0	1.4	0	0	1.6	76.4
	Right	1.1	7.5	4.1	3.1	4.6	0	0	1.1	0	78.4
Bilateral Superior Facetectomy	Left	2.1	4.1	7.6	5.7	0	0	0	0	1.6	78.9
	Right	1.4	6.4	5.2	2.8	0	0	0	1.1	0	83.2

left and right axial rotation (Figure 7c), the ICR experiences a 0.23mm shift in the medial and lateral directions, respectively, after spinous ligament removal. After the bilateral inferior facetectomy is simulated, a shift occurs by 0.17mm laterally and 0.65mm anteriorly in left axial rotation, and 0.13mm medially and 1mm anteriorly in right axial rotation. After the bilateral superior facetectomy is simulated; a shift of 0.24mm and 0.09mm respectively occur medially and anteriorly in left axial rotation, and a shift of 1.49mm and 0.63mm respectively occur medially and anteriorly in right axial rotation.

3.3 Functional unit load distribution

3.3.1 Flexion and Extension

In flexion (Table 6), 56 percent of the total load is initially borne by posterior ligaments, however, approximately 76 percent of the total load at the maximally applied moment were carried by the IVD, ITL, and the LF, at approximately 44 percent, 17 percent, and 16 percent load distribution respectively; the spinous ligaments bore approximately 18 percent. When the spinous ligaments were removed, the total load distribution among the 3 components accounted for approximately 92 percent of the total load. The largest overall increase in load distribution occurred when the ligamentum flavum was removed, leading to a 19.4 percent increase in the amount of load borne by the intertransverse ligament.

In extension, approximately 88 percent of the total load at maximum applied moment is borne by the facet joint and intervertebral disc. However, load redistribution is only seen when the bilateral inferior and superior facetectomies are conducted, increasing by approximately 17 percent and 0.5 percent respectively within the intervertebral disc; meanwhile, load distribution in the facets drop respectively by 21 percent and 0.4 percent. The CCJ and CTV showed an increase of approximately 1.6 percent and 2.4 percent, respectively, in load distribution after the bilateral inferior facetectomy was conducted. The absence of compression stiffness within both spinous ligaments and the ligamentum flavum create negligible change in the load distribution following removal.

3.3.2 Left and Right Lateral Bending

In left lateral bending (Table 7), approximately 79 percent of the load distribution is borne by the IVD intact and experiences an increase in load bearing to approximately 82 percent after the bilateral inferior facetectomy is conducted, due to the left facet bearing only 2.5 percent of the total load prior to removal. Negligible load by the facet is borne during subsequent steps. The right ITL bears approximately 7.6 percent of total load with negligible distribution change during release. In right lateral bending, the IVD bears approximately 70 percent of the load distribution intact and increases by approximately 3 percent after the bilateral superior facetectomy is simulated. The left ITL bears approximately 6 percent of total load and negligibly changes

throughout release. Load borne by the right CCJ bears approximately 12 to 13 percent, driven by contact between the rib head and T7. The distributions of the other CV joint components are not as variable between left and right lateral bending, bearing less than 7 percent total load overall.

3.3.3 Left and Right Axial Rotation

In left axial rotation (Table 8), approximately 64 percent of the load distribution is borne by the intervertebral disc in the intact model and increases to approximately 76 percent and 79 percent after the bilateral inferior and superior facetectomies are respectively conducted. The left and right FJ bear approximately 14 percent and 3.6 percent total load respectively prior to the inferior facet removal, then drop to zero and 1.4 percent respectively following the bilateral inferior facetectomy. The CV joint components bear no more than 6.4 percent of the total load prior to facet removal, seen by the left CTV, which experiences an approximately 1.5 percent maximum increase. In right axial rotation, approximately 67 percent load distribution is borne by the IVD; this increases to approximately 79 percent and 83 percent respectively after the bilateral inferior and superior facetectomies. As with the left axial rotation, the change in load distribution is evidenced by the left and right FJ bearing approximately 14 percent and 6 percent load respectively prior to removal. After the bilateral inferior facetectomy stage the load distribution on the left and right FJ drop to 4.6 percent and zero respectively. The CV joint components see a maximum increase of 1.9 percent load distribution by the left CTV after facet removal; however, prior to facet removal, the components bear no more than approximately 6 percent. The load borne by the left and right ITL was small in comparison throughout all removal steps, seeing less than 2 percent throughout the entire procedure. A small load sharing percentage of approximately 0.64 percent is borne by the ISL in right axial rotation prior to removal.

4 Discussion

Patient-specific surgical planning can be a challenging feat due to variability in symptomatic profiles. The nonlinearities of vertebral geometry and wide-ranging characterization of soft tissue (Wang et al 2014; Lafon et al 2010) can affect clinical decisions on how to optimally address spinal deformities. An anatomic-based load distribution assessment within a spinal FE model can highlight the contribution individual soft tissues make toward spinal flexibility through external moment resistance. In turn, insight can be provided on the kinematic effects serial anatomic release presents in spinal segments, such as shifts in ICR and load bearing to other components, potentially assisting surgeons to achieve desired deformity corrections without compromising rotational stability.

Posterior correction procedures such as the Ponte osteotomy (Samdani et al 2015; Ponte et al 2018), through resectioning of spinal ligaments and

facet joints at a spinal deformity apex, have gained interest within the surgical community because of their superior correction outcomes. More aggressive techniques, such as a Pedicle Subtraction osteotomy or Vertebral Column resectioning (Kose et al 2017), may be required to obtain necessary correction for patients with large kyphoscoliotic curves. Despite the advances in column correction procedures, minimizing intra- and post-operative risks presented during spinal destabilization remains challenging. For example, facet removal to correct kyphosis during a Ponte osteotomy could lead to a foraminal height decrease and, thus, neural impingement. Kose et al (2017) recommended that laminectomies during a pedicle subtraction osteotomy be extended to one level above and below the apex to avoid spinal cord buckling. Other risks such as blood loss are posed during osteotomy procedures. While a load-bearing assessment primarily highlights the potential flexibility gains during spinal resectioning, it is imperative these operative limitations be considered to minimize patient risk.

To the authors' knowledge, the study is the first to use the ICR for thoracic posterior release. In flexion, the anterior shift of the ICR position during each resection step agrees with clinical observations regarding posterior release (Ponte et al 2018). A significant shift in ICR position upon spinous ligament removal confirms their importance in spinal column stabilization, whose resistance is driven by the moment arm and posterior positioning (Sharma et al 1995). Previous in-vitro (Wilke et al 2020) and FE model (Little and Adam 2011b) studies did not draw that conclusion potentially due to the lower moment magnitudes applied (2.5 and 2 Nm versus 5 Nm), consequentially affecting the strain seen from those ligaments. In addition, the high load bearings of the ligamentum flavum and intertransverse ligaments could be attributed to high thickness and stiffness characterizations present within the thoracic spine (White and Panjabi 1990, p.20,22-23). As such, removal of the ligamentum flavum contributed to a significant ICR shift. Except for flexion, where most load sharing took place within the posterior ligaments, the study confirms the load bearing significance of the intervertebral disc throughout all rotations and resection steps. The CV joint, overall, did not contribute significantly to the load distribution of the functional unit, possibly due to the open bilateral configuration of the ribs. Additionally, the T7-T8 FE model rotations in three anatomic planes amount to 6.9°, 4.4°, and 3.4°, versus 1.9° (flexion and extension), 1.7° (one-side lateral bending), and 2.3° (one-side axial rotation) respectively when compared with in-vivo data (Pan et al 2018). With an intact ribcage configuration present, however, stiffer behavior could be reinforced (Liebsch and Wilke 2020).

Significant shifts in kinematic behavior were exhibited after the inferior and superior facets were removed, particularly in axial rotation. As a result of the capsular ligament being absent following the bilateral inferior facetectomy, the absence of load distribution alternates based on the rotation direction, supplemented by contact between the superior and remaining inferior facets. The inferior facet removal saw more correction overall as most of

the facet is removed, and smaller correction amounts after the superior facets were removed. This finding agrees with the results from the in-vitro study by Holewijn et al (2015). Superior facet removal may be utilized on a scoliosis patient to achieve further correction if residual pressure between inferior and superior facets complicates the surgery. Thus, an FE model with scoliosis may predict greater correction following removal of the superior facets. The setup for the bilateral inferior facetectomy was driven by general practice of removing the inferior facet up to the transverse process bottom during a Ponte osteotomy (Ponte et al 2018). However, the amounts of the facet left upon release may vary based on surgeon experience and facet orientation.

The scarcity of ligament data in the literature was a primary limitation of the study. Very few studies offer material ligament data for direct application to the thoracic spine (Chazal et al 1985) compared to the lumbar region, where ligament data is more available and is stiffer compared to thoracic ligaments. Thus, a compromise was made to scale ligament stiffnesses by cross-sectional areas appropriate for the mid-thoracic spine. In comparing the rotations from the FE model with the abridged experimental (Wilke et al 2020) sectioning sequence of spinal anatomy most pertinent to the Ponte osteotomy, the functional unit with posterior ligament properties chosen performed well in right lateral bending, left axial rotation, and flexion up to the spinous ligament sectioning. Compliance, however, was exhibited in extension and flexion rotations upon ligamentum flavum and facet joint release, leaving the longitudinal ligaments intact. The anterior and posterior longitudinal ligaments in the mid-thoracic regions are thicker relative to other spinal regions. Thus, the compliance may be explained by insufficient capture of width and thickness measurements using one-dimensional ligaments and may be better represented using two- or three-dimensional formulations.

Motion resistance by the FE model facet joints was demonstrated in right lateral bending and left axial rotation, producing the only significant change in RoM during sequential release. They are also a prominent contributor to motion resistance in extension, which exhibited compliant behaviour relative to the experiment. Historically, facet joints have been modeled utilizing available contact algorithms in FE codes; the methods in which facets have been modeled vary greatly (Mengoni 2021) and could affect key parameters such as RoM and facet joint forces (Zander et al 2017). The nonzero moment percentages reported for the facets indicate they engage in contact; however, the penalty algorithm alone may fail to sufficiently capture facet joint mechanics, which is realistically a fluid-solid interaction between synovial fluid and cartilage layers. Thus, to enhance facet modeling, parameters such as contact gaps and facet capsule characterization should be explored thoroughly; such parameters may affect load distributions calculated in spine models. Explicit representation of the synovial fluid may also be needed to enhance facet incompressibility.

The load distribution findings presented assume that the FE model moves within a plane and that negligible coupling takes place. Future work may investigate the effects of out-of-plane coupling on load distribution within the

spinal column. In addition, the load distribution behavior is valid for the provided set of ligament properties and the sectioning sequence applied for a Ponte osteotomy. Both spinal flexibility and deformity are known to vary on a patient-specific basis (Lafon et al 2010; Lamarre et al 2009); thus, the load distribution behavior may be altered based on the patient or the section sequence performed. The analyses presented assumed no ligament pretension as previous FE analyses assumed forces less than 10N (Meijer 2011). However, ligament pretension has been attributed to changes in lordosis angles (Heuer et al 2007) during ligament sectioning in the lumbar spine, not measured in these analyses, and will be further assessed in future FE model studies. Lastly, the load distribution presented was valid for one mid-thoracic segment. As intervertebral stiffness varies throughout the spinal column (Panjabi and White 1990, p. 47), load distribution within different regions of the spine should be investigated as it can influence the level of surgical correction achievable.

5 Conclusion

A load distribution assessment has been performed on a FE model of a thoracic functional unit for potential application to surgical planning. Ligament properties were chosen and utilized based on available in-vitro data, qualitative descriptions of ligaments within the thoracic spine, and comparability with available experimental data. The simulated posterior release, through kinematic and load distribution changes, highlight components, like the intervertebral disc and facet joints, which are crucial to stabilization during serial removal. Also emphasized is the importance of moment arm, through the ICR, in determining the resistance levels that components exert during segmental rotation. A surgeon may collectively utilize these variables to achieve desired post-surgical outcomes while decreasing risk for their patients.

Declarations

Funding. The following study was supported by Children’s Hospital of the King’s Daughters in Norfolk, VA under Grant number 7376 and the SMART Scholarship Program received by Michael Polanco.

Author’s Contributions. Michael Polanco was primarily involved in building the finite element model and conducting the anatomic load assessment. Both Sebastian Bawab and Stacie Ringleb supervised Mr. Polanco’s work and provided appropriate guidance for completion of the work. James Bennett is an orthopedic surgeon at Children’s Hospital of the King’s Daughters in Norfolk, VA USA and provided clinical guidance for Mr. Polanco’s work. Michel Audette serves as the Principal Investigator for a Scoliosis surgical planning research grant which includes a Finite Element modeling counterpart. Austin Tapp has been working under the same research grant. All these individuals were involved with a thorough review of the manuscript being submitted and agree with the findings and content documented.

Conflict of Interest. No conflicts of interest are declared by any of the authors.

References

Aira J, Guleyupoglu B, Jones D, Koya B, Davis M, Gayzik FS (2019) Validated thoracic vertebrae and costovertebral joints increase biofidelity of a human body model in hub impacts. *Traffic Inj Prev.* 20(sup2): S1-S6. Accompanied by online supplement.

Asher MA, Burton DC (2006) Adolescent idiopathic scoliosis: natural history and long-term treatment effects. *Scoliosis.* 1(1):2.

Chazal J, Tanguy A, Bourges M, Gaurel G, Escande G, Guillot M, Vanneuville G (1985) Biomechanical properties of spinal ligaments and a histological study of the supraspinal ligament in traction. *J Biomech.* 18(3):167-176.

He C, Wong MS (2018) Spinal flexibility assessment on the patients with Adolescent Idiopathic Scoliosis: a literature review. *Spine (Phila Pa 1976).* 43(4): E250-E258.

Heuer F, Schmidt H, Klezl Z, Claes L, Wilke HJ (2007) Stepwise reduction of functional spinal structures increase range of motion and change lordosis angle. *J Biomech.* 40(2):271-280.

Holewijn RM, Schlosser TPC, Bisschop A, van der Veen AJ, Stadhouders A, van Royan BJ, Castelein RM, de Kleuver M (2015) How does spinal release and Ponte osteotomy improve spinal flexibility? The law of diminishing returns. *Spine Deformity.* 3:489-495.

Jiang HX, Raso JV, Moreau MJ, Russell G, Hill DL, Bagnall KM (1994) Quantitative morphology of the lateral ligaments of the spine - assessment of their importance in maintaining lateral stability. *Spine.* 19(23):2676-2682. English.

Kose KC, Bozduman O, Yenigul AE, Iğrek S (2017) Spinal osteotomies: indications, limits and pitfalls. *EFORT open reviews.* 2(3): 73-82.

Lafon Y, Steib JP, Skalli W (2010) Intraoperative three-dimensional correction during in situ contouring surgery by using a numerical model. *Spine.* 35(4):453-459.

Lamarre ME, Parent S, Labelle H, Aubin CE, Joncas J, Cabral A, Petit Y (2009) Assessment of spinal flexibility in adolescent idiopathic scoliosis: suspension versus side-bending radiography. *Spine (Phila Pa 1976).* 34(6):591-597.

Lenke LG, Edwards CC, Bridwell KH (2003) The Lenke classification of Adolescent Idiopathic Scoliosis: how it organizes curve patterns as a template to perform selective fusions of the spine. *Spine*. 28(20S): S199-S207.

Liebsch C, Wilke HJ (2020) Rib Presence, Anterior Rib Cage integrity and segmental length affect the stability of the thoracic spine: An in vitro study. *Front Bioeng Biotechnol*. 8(46):1-10.

Little JP, Adam CJ (2011a) Patient-specific computational biomechanics for simulating adolescent scoliosis surgery: Predicted vs clinical correction for a preliminary series of six patients. *International Journal for Numerical Methods in Biomedical Engineering*. 27:347-356.

Little JP, Adam CJ (2011b) Effects of surgical joint destabilization on load sharing between ligamentous structures in the thoracic spine-a finite element study. *Clin Biomech (Bristol, Avon)*. 26:895-903.

Lo HJ, Chen HM, Kuo YJ, Yang SW (2020) Effect of different designs of interspinous process devices on the instrumented and adjacent levels after double-lumbar decompression surgery: a finite element analysis. *PLoS One*. 15(12):1-13.

Meijer GJ (2011) Development of a non-fusion scoliosis correction device: numerical modelling of scoliosis correction. [dissertation]. Stichting Technologische Wetenschappen: Universiteit of Twente.

Majdoulina Y, Aubin CE, Sangole A, Labelle H (2009) Computer simulation for the optimization of instrumentation strategies in adolescent idiopathic scoliosis. *Med Biol Eng Comput*. 47(11):1143-1154.

Mengoni M (2021) Biomechanical modelling of the facet joints: a review of methods and validation processes in finite element analysis. *Biomech Model Mechanobiol*. 20(2):389-401.

Naserkhaki S, Arjmand N, Shirazi-Adl A, Farahmand F, El-Rich M (2018) Effects of eight different ligament property datasets on biomechanics of a lumbar L4-L5 finite element model. *J Biomech*. 70:33-42.

Naserkhaki S, Jaremko JL, Adeeb S, El-Rich M (2016) On the load-sharing along the ligamentous lumbosacral spine in flexed and extended postures: Finite element study. *J Biomech*. 49(6): 974-982.

Oda I, Abumi K, Cunningham BW, Kaneda K, McAfee PC (2002) An in vitro human cadaveric study investigating the biomechanical properties of the thoracic spine. *Spine (Phila Pa 1976)*. 27(3): E64-70.

Pan F, Firouzabadi A, Reitmaier S, Zander T, Schmidt H (2018) The shape and mobility of the thoracic spine in asymptomatic adults – A systematic review of in vivo studies. *Biomechanics*. 78:21-35.

Panzer M, Cronin D (2009) C4–C5 segment finite element model development, validation, and load-sharing investigation. *Biomechanics*. 42:480-490.

Pearcy MJ, Bogduk N (1988) Instantaneous axes of rotation of the lumbar intervertebral joints. *Spine (Phila Pa 1976)*. 13(9):1033-1041.

Polanco M, Ringleb S, Audette M, Kakar R, Bawab S (2022) A comparison of intervertebral ligament properties utilized in a thoracic spine functional unit through kinematic evaluation. *Computer Methods in Biomechanics and Biomedical Engineering*. doi: 10.1080/10255842.2022.2115293.

Ponte A, Orlando, G., Siccardi, GL (2018) The true Ponte osteotomy-by the one who developed it. *Spine Deformity*. 6.

Samdani AF, Bennett JT, Singla AR, Marks MC, Pahys JM, Lonner BS, Miyanji F, Shah SA, Shufflebarger HL, Newton PO et al (2015) Do Ponte osteotomies enhance correction in Adolescent Idiopathic Scoliosis? An analysis of 191 Lenke 1A and 1B curves. *Spine Deformity*. 2:483-488.

Schlager B, Niemeyer F, Liebsch C, Galbusera F, Boettinger J, Vogeles D., Wilke HJ (2018) Influence of morphology and material properties on the range of motion of the costovertebral joint – a probabilistic finite element analysis. *Computer Methods in Biomechanics and Biomedical Engineering*. 21(14) :731-739.

Schmidt H, Heuer F, Simon U, Kettler A, Rohlmann A, Claes L, Wilke HJ (2006) Application of a new calibration method for a three-dimensional finite element model of a human lumbar annulus fibrosus. *Clin Biomech (Bristol, Avon)*. 21(4):337-344.

Schmidt H, Heuer F, Claes L, Wilke HJ (2008) The relation between the instantaneous center of rotation and facet forces-a finite element analysis. *Clinical Biomechanics*. 23:270-278.

Sharma M, Langrana NA, Rodriguez J (1995) Role of ligaments and facets in lumbar spinal stability. *Spine (Phila Pa 1976)*. 20(8):887-900.

Shirazi-Adl A, Ahmed AM, Shrivastava SC (1986) Mechanical response of a lumbar motion segment in axial torque alone and combined with compression. *Spine (Phila Pa 1976)*. 11(9):914-927.

Stokes IA (1994) Three-dimensional terminology of spinal deformity. A report presented to the Scoliosis Research Society by the Scoliosis Research Society

Working Group on 3-D terminology of spinal deformity. *Spine* (Phila Pa 1976). 19(2):236-248.

Vergari C, Ribes G, Aubert B, Adam C, Miladi L, Ilharreborde B, Abelin-Genevois K, Rouch P, Skalli W (2015) Evaluation of a patient-specific finite element model to simulate conservative treatment in Adolescent Idiopathic Scoliosis. *Spine Deform.* 3(1):4-11.

Wang W, Baran GR, Betz RR, Samdani AF, Pahys JM, Cahill PJ (2014) The use of finite element models to assist understanding and treatment for scoliosis: a review paper. *Spine Deform.* 2(1):10-27.

White AA, Panjabi MM (1990) *Clinical Biomechanics of the Spine*. 2nd ed. Philadelphia, PA: Lippincott, Williams, and Wilkins. p.20, 22-23, 47.

Wilke HJ, Grundler S, Ottardi C, Mathew CE, Schlager B, Liebsch C (2020) In vitro analysis of thoracic spinal motion segment flexibility during stepwise reduction of all functional structures. *European Spine Journal.* 29(1):179-185. English.

Wilke HJ, Wenger K, Claes L (1998) Testing criteria for spinal implants-recommendations for the standardization of in vitro stability testing of spinal implants. *Eur Spine J.* 7:148-154.

Wu CC, Jin HM, Yan YZ, Chen J, Wang K, Wang JL, Zhang ZJ, Wu AM, Wang XY (2018) Biomechanical role of the thoracolumbar ligaments of the thoracic posterior complex: a finite element analysis. *World Neurosurgery.* 112:e125-e133.

Zander T, Dreischarf M, Timm AK, Baumann WW, Schmidt H (2017) Impact of material and morphological parameters on the mechanical response of the lumbar spine - a finite element sensitivity study. *J Biomech.* 53:185-190.

Zhang Z, Fogel GR, Liao Z, Sun Y, Liu W (2018) Biomechanical analysis of lateral lumbar interbody fusion constructs with various fixation options: based on a validated finite element model. *World Neurosurgery.* 114:e1120-e1129.

6 Figures

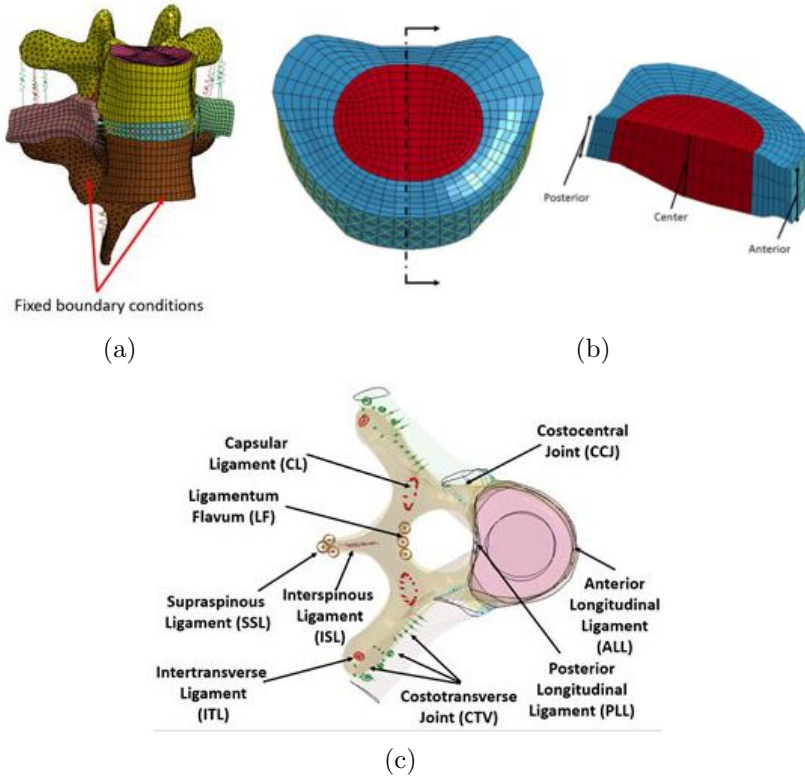


Fig. 1: (a) T7-T8 Finite element model; (b) Intervertebral Disc with cross-section view; (c) Transparent axial view with ligaments and joints labeled.

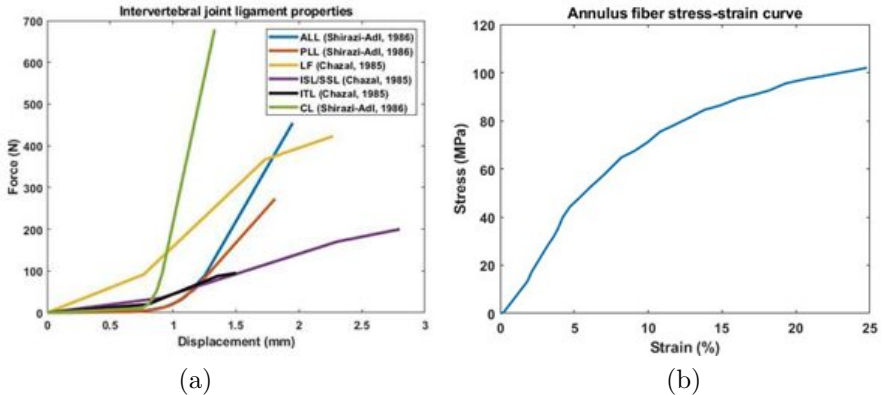


Fig. 2: (a) Ligament stiffness curves and their sources; (b) Annulus Fiber Stress-Strain curve from Shirazi-Adl (1986)

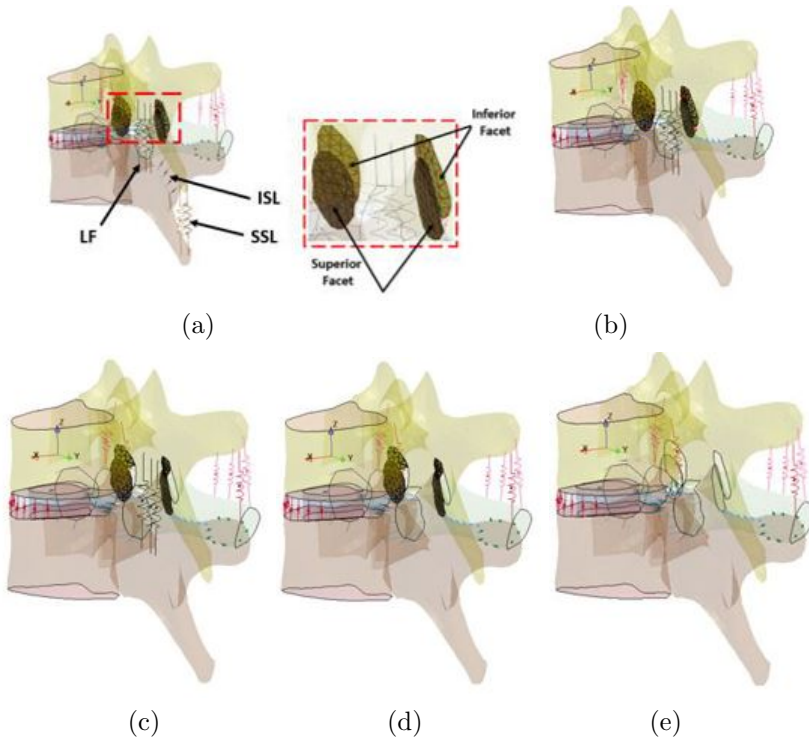


Fig. 3: The five model configurations corresponding to the steps of a Ponte osteotomy: (a) Step 1: An intact configuration. Components removed in subsequent steps are labeled; (b) Step 2: Removal of the Spinous Ligaments (SSL and ISL); (c) Step 3: Bilateral inferior facetectomy; (d) Step 4: Ligamentum Flavum (LF) removal; (e) Step 5: Bilateral superior facetectomy.

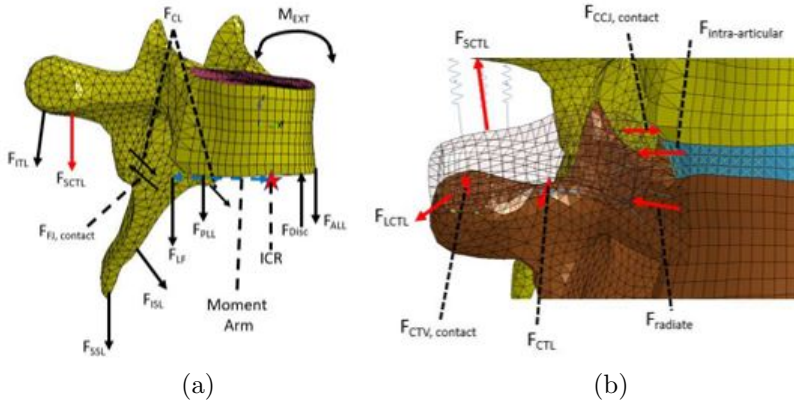
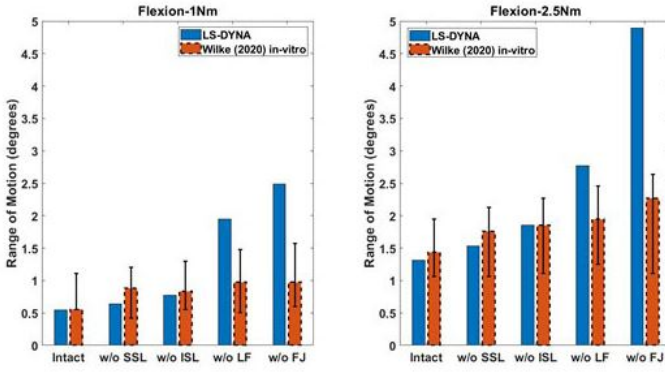
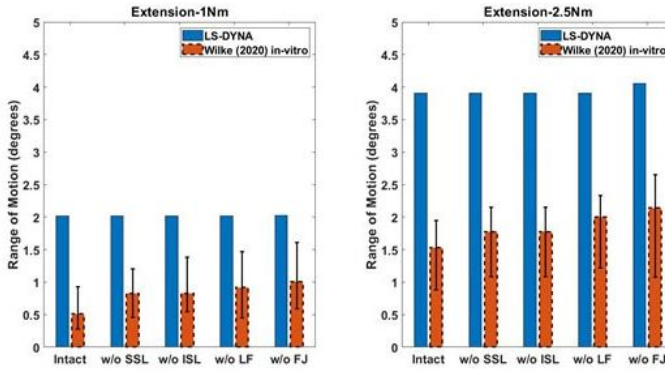


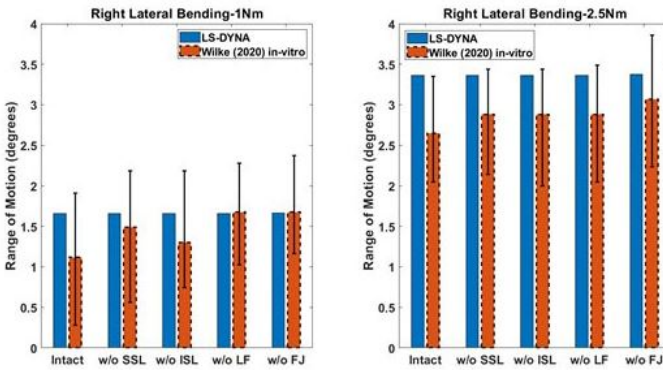
Fig. 4: (a) Free-body diagram of intervertebral spine components with moment arm; (b) Free-body diagram of CV joint components (red arrow depiction).



(a)



(b)



(c)

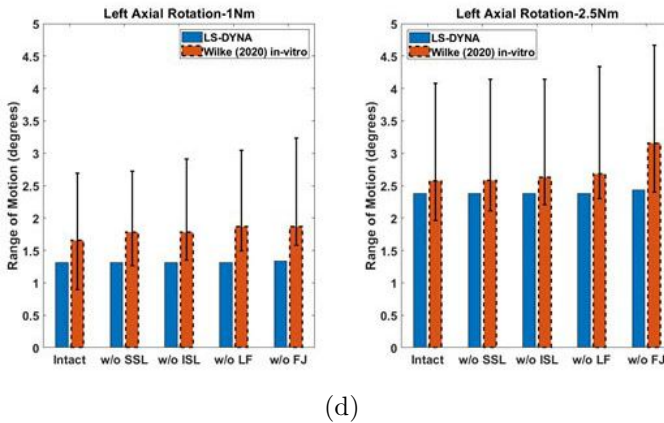


Fig. 5: Stepwise ligament removal (a) Flexion; (b) Extension; (c) Right Lateral Bending; (d) Left Axial Rotation.

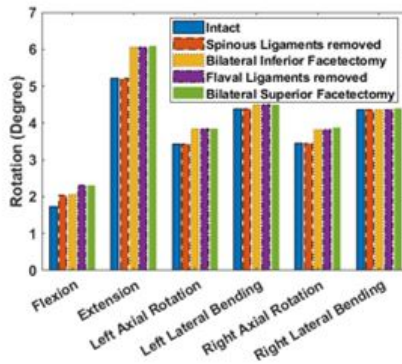
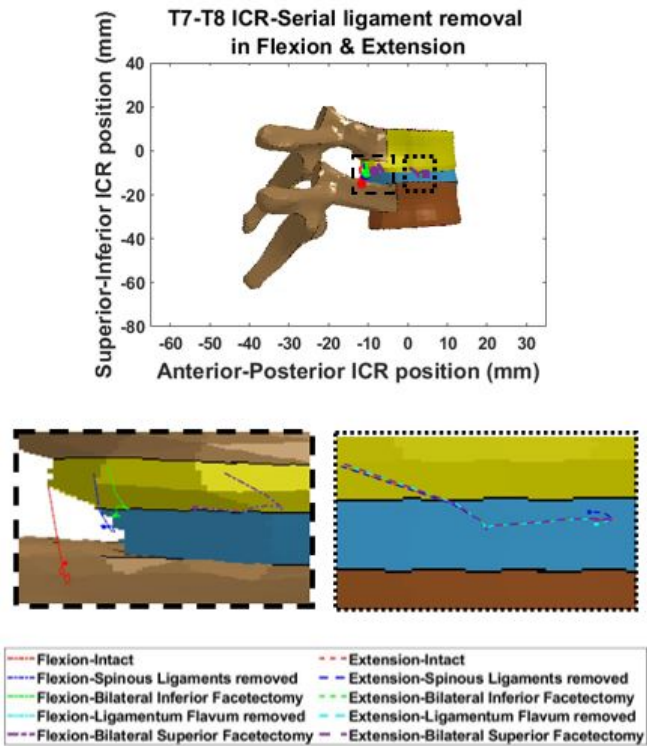
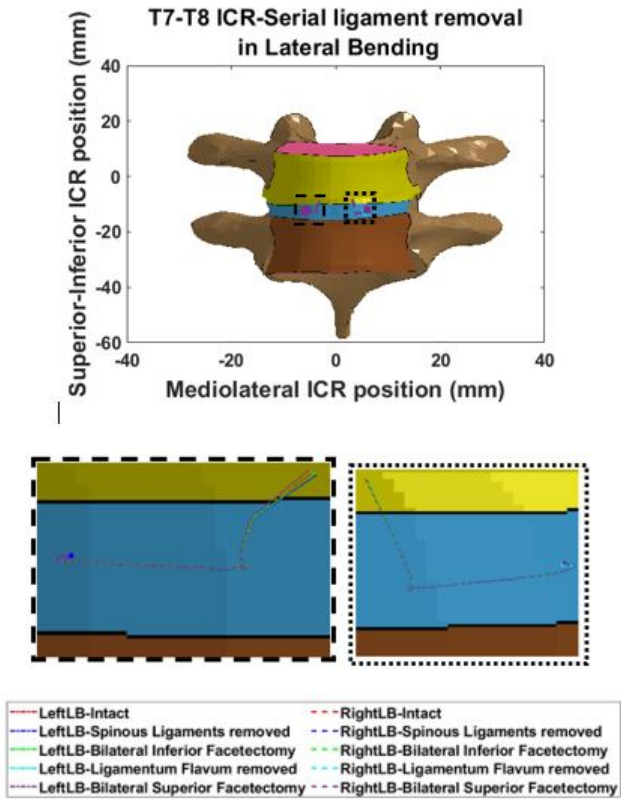


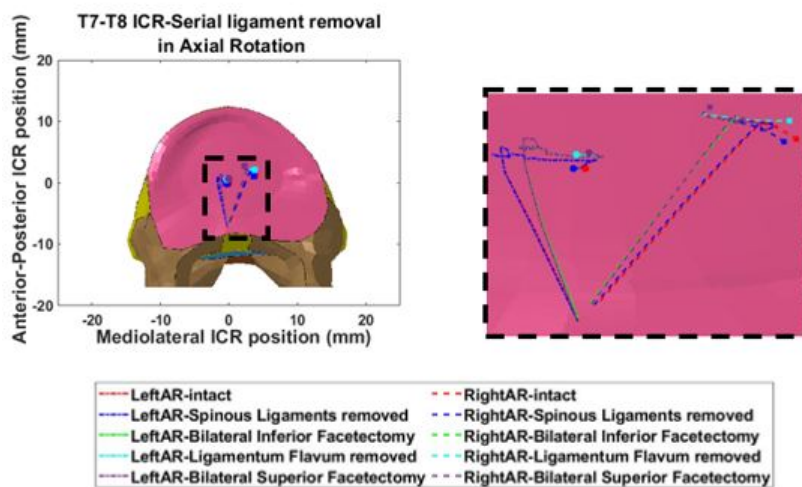
Fig. 6: Bidirectional RoM of functional unit registered at the maximum applied moment (± 5 N-m).



(a)



(b)



(c)

Fig. 7: ICR traces with solid markers depicting the rotation center at maximum load. (a) Flexion-Extension; (b) Left-Right Lateral Bending; (c) Left-Right Axial Rotation..

Appendix A

Resultant forces and stresses from ligaments, facets, and IVD

Table A1: Sagittal plane force resultant values in Newtons for ligaments and facet joints at 5 N-m

		ALL	CCJ	CTV	FJ	ITL	LF	ISL	SSL	PLL
Intact	Flexion	0	6.6	11.3	6.5	33.5	48.8	14.2	13.4	0
	Extension	3.5	14.2	11.8	37.1	0	0	0	0	0
ISL and SSL removed	Flexion	0	9.3	12.9	10.3	43.3	62.9	0	0	0
	Extension	3.5	14.2	12	37.1	0	0	0	0	0
Bilateral Inferior Facetectomy	Flexion	0	11.6	12.9	0	46.9	65.2	0	0	0
	Extension	4	20.1	15.7	9.7	0	0	0	0	0
LF removed	Flexion	0	12.7	15.9	0	82.4	0	0	0	0
	Extension	4	20.1	15.7	9.7	0	0	0	0	0
Bilateral Superior Facetectomy	Flexion	0	13	15.9	0	82.4	0	0	0	0
	Extension	4	19.6	15.8	0	0	0	0	0	0

Table A2: Lateral Bending force resultant values in Newtons for ligaments and facet joints at 5 N-m

		CCJ- Left	CCJ- Right	CTV- Left	CTV- Right	FJ- Left	FJ- Right	ITL- Left	ITL- Right
Intact	Left	6.9	4.3	4.9	8.4	7.6	0	0	16.1
	Right	2.3	32.7	5.3	9.7	0	5.1	13	0
ISL and SSL removed	Left	6.9	4.3	4.9	8.4	7.6	0	0	16.1
	Right	2.3	32.7	5.3	9.7	0	5.1	13	0
Bilateral Inferior Facetectomy	Left	7.8	4.1	5.6	8.1	0	0	0	15.3
	Right	2.3	32.6	5.3	9.7	0	5.1	13	0
LF removed	Left	7.8	4.1	5.6	8.1	0	0	0	15.3
	Right	2.3	32.7	5.3	9.7	0	5.1	13	0
Bilateral Superior Facetectomy	Left	7.8	4.1	5.6	8.1	0	0	0	15.3
	Right	2.4	30.3	5.3	9	0	0	12.8	0

Table A3: Axial rotation force resultant values in Newtons for ligaments and facet joints at 5 N-m

		CCJ- Left	CCJ- Right	CTV- Left	CTV- Right	FJ- Left	FJ- Right	ISL	ITL- Left	ITL- Right
Intact	Left	6.2	10.2	8.5	8.9	27.7	9.2	0	0	1.1
	Right	4.8	17.2	4	3.7	28.6	9.5	1.4	0.47	0
ISL and SSL removed	Left	6.2	11.9	8.5	8.7	27.8	9.3	0	0	1.1
	Right	4.9	17.3	4.1	3.7	28.2	10.1	0	0.7	0
Bilateral Inferior Facetectomy	Left	8.2	12.8	10.4	9.5	0	3.4	0	1.8	0
	Right	5.4	20.6	6.5	4	17.9	0	0	1.2	0
LF removed	Left	8.2	12.8	10.4	9.5	0	3.4	0	1.8	0
	Right	5.4	20.6	6.4	4	17.8	0	0	1.2	0
Bilateral Superior Facetectomy	Left	8.2	11.7	10	9.6	0	0	0	1.8	0
	Right	6.2	17.4	7.7	3.5	0	0	0	1.2	0

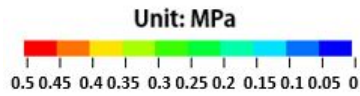
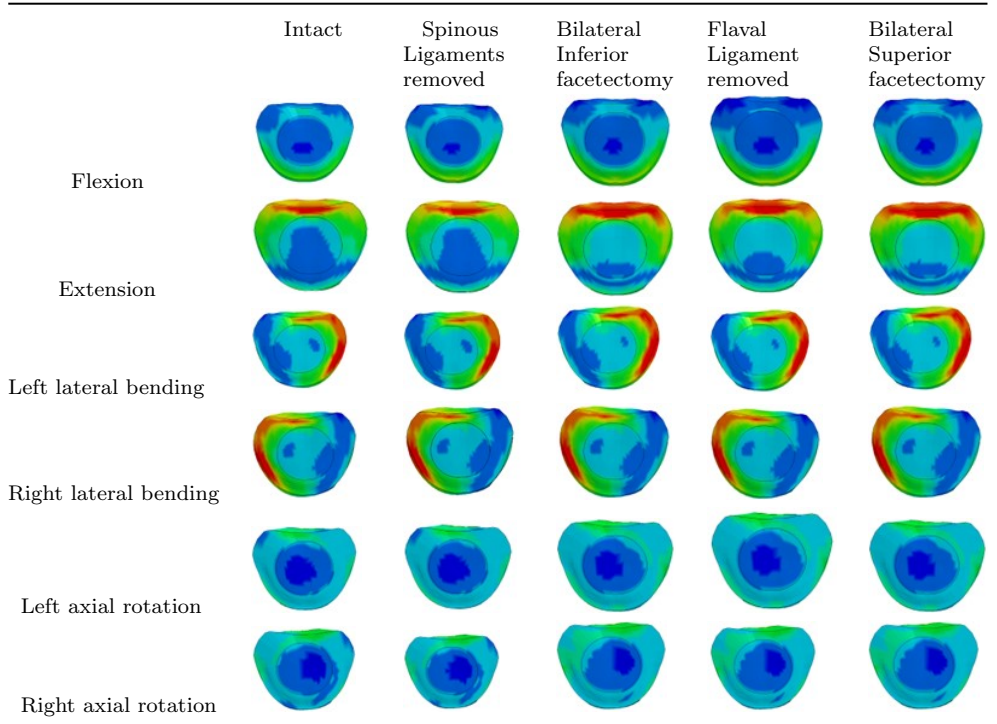
Table A4: Intervertebral Disc stresses-transverse view

Table A5: Annulus fiber forces-transverse view